Journal of Micromechanics and Microengineering

PAPER

Measurements of residual stresses in the Parylene C film/silicon substrate using a microcantilever beam

To cite this article: Jyun-Siang Peng *et al* 2013 *J. Micromech. Microeng.* **23** 095001

View the article online for updates and enhancements.

Related content

- Thermal stress analyses of multilayered films on substrates and cantilever beams for micro sensors and actuators
C H Hsueh, C R Luttrell and T Cui
- Fabrication of thin SU-8 cantilevers
Stephan Keller, Daniel Haefliger and Anja Boisen
- Investigating thin film stresses in stacked silicon dioxide/silicon nitride structures
Omar Zohni, Gregory Buckner, Taeyun Kim et al.

Recent citations

- Size-dependent electro-thermo-mechanical analysis of multilayer cantilever microactuators by Joule heating using the modified couple stress theory
Zou-Qing Tan and Yang-Chun Chen
- A closed-form solution for thermal stresses of structures using generalized variational principles
Zou-Qing Tan *et al*
- Study on the Vibration of Optically Excited Microcantilevers Under Fractional-Order Thermoelastic Theory
Yaqin Song *et al*

IOP ebooks™

Bringing you innovative digital publishing with leading voices to create your essential collection of books in STEM research.

Start exploring the collection - download the first chapter of every title for free.

This content was downloaded from IP address 140.114.57.227 on 12/02/2019 at 09:09

IOP PUBLISHING JOURNAL OF MICROMECHANICS AND MICROENGINEERING

J. Micromech. Microeng. **23** (2013) 095001 (7pp) doi:10.1088/0960-1317/23/9/095001

Measurements of residual stresses in the Parylene C film/silicon substrate using a microcantilever beam

Jyun-Siang Peng[1], Weileun Fang[2], Hung-Yi Lin[3], Chun-Hway Hsueh[4] and Sanboh Lee[1,5]

[1] Department of Materials Science and Engineering, National Tsing Hua University, Hsinchu 30013, Taiwan

[2] Department of Power Mechanical Engineering, National Tsing Hua University, Hsinchu 30013, Taiwan

[3] Mechanical and System Research Laboratories, Industrial Technology Research Institute, Chutung, Hsinchu 31040, Taiwan

[4] Department of Materials Science and Engineering, National Taiwan University, Taipei 10617, Taiwan

E-mail: sblee@mx.nthu.edu.tw

Received 22 April 2013, in final form 1 July 2013
Published 1 August 2013
Online at stacks.iop.org/JMM/23/095001

Abstract
A series of Parylene C film/silicon substrate bilayer microcantilever beams were fabricated by microelectromechanical processes for the study of residual stresses. The Parylene C films of 2 μm thickness were deposited on the Si substrates with various thicknesses. After deposition at room temperature, deflection of the beam was observed with deposited Parylene C on the concave side. While Parylene C has a higher coefficient of thermal expansion than Si, this deflection is believed to result from the thermal mismatch between Parylene C and Si, and the temperature of monomer gas (which is formed at 690 °C) flowing across the sample could be higher than 25 °C. It is estimated to be 73 °C based on the fitting of the curvature versus substrate thickness relation between the measurements and analytical solutions. In this case, Parylene C films are subjected to tension. In addition, the residual stress in the Parlyene C film decreases with decreasing substrate thickness.

(Some figures may appear in colour only in the online journal)

1. Introduction

Microcantilever beams have been integrated into microsystems and have demonstrated a wide range of novel physical, chemical and biological applications [1–3]. Therefore, the microcantilevers have attracted much attention in research and industrial sectors in the past few decades [4–8]. Owing to the low cost, low driving power and large deflection, microcantilevers have been applied in microprobes, optical switch and infrared gas spectrometers [9–11]. However, the majority of these cantilevers are fabricated by surface micromachining techniques which, in turn, result in a residual stress gradient in the system [12]. These residual stresses could be attributed to thermal mismatch between the film and the substrate [13, 14], defects in the film (impurities, dislocations, grain boundaries and voids) during film deposition [15–17], lattice mismatch between two crystalline materials [18] and/or the surface stresses in the film [19]. As a result, the measurement of residual stresses has become an intrigue topic. In order to characterize the complicated stress issues in different industrial systems, several methods, such as a bilayer cantilever [20, 21], displacements of various microstructures [22, 23], buckling lengths and radius [24, 25], resonance frequency [26] and pull-in voltages [27] have been developed. Among these methods, the method of bilayer cantilever is most widely used to measure residual stresses in a thin film because of its ease in analysis.

Poly(p-xylylene) (Parylene) and its derivatives are inert, non-degradable and biocompatible materials with superior physical and mechanical properties [28, 29], and hence

[5] Author to whom any correspondence should be addressed.

 © 2013 IOP Publishing Ltd Printed in the UK & the USA

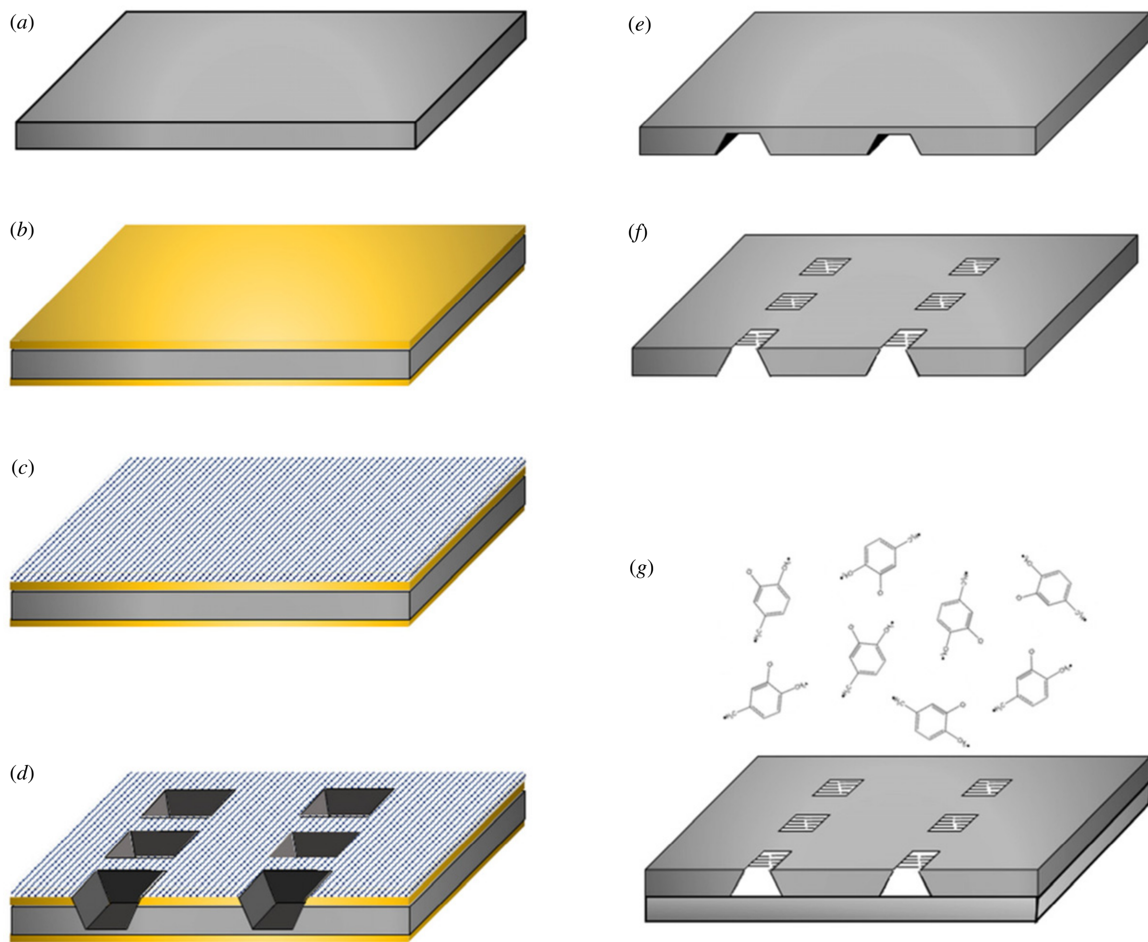

Figure 1. Schematics showing (*a*) a pristine Si wafer, (*b*) Si_3N_4 deposited on both sides of the Si wafer as passive layers, (*c*) FH 6400 positive photoresist coated on the backside for further lithography, (*d*) etching of Si_3N_4 and Si by RIE and KOH wet etching, respectively, (*e*) removal of the Si_3N_4 passive layer by RIE etching, (*f*) transfer of the microcantilever beam patterns on the top side and deep etching of Si, and (*g*) deposition of Parylene C monomers on the composite wafer system.

they have been extensively used in medical devices for coating implantable components [30] and in electrical devices as an insulating and bonding material [31, 32]. Among them, poly-(monochloro-*p*-xylylene) (Parylene C) has a lower process temperature as well as compatibility with the standard microfabrication process [29]. Thus, it has become a potential candidate for the application of medical devices. Nevertheless, the adhesion force between Parylene C and the silicon substrate is weak, and the residual stresses could cause device failure. For this reason, the measurement of the residual stresses in the Parylene C/silicon bilayer cantilever system to provide parameters for the device design is crucial. The analysis of residual stresses in a bilayer system was first studied by Stoney [33] by considering a thin film with a negligible thickness on a thick substrate. This analysis was subsequently improved by many others by considering a finite thickness of the film and extending to the multilayer system [34–37].

On the other hand, methods other than the microcantilever beam were performed to measure the intrinsic stress of the Parylene C film [38–41]. Using the load-deflection tests, Yang *et al* [38] found the Young modulus and residual stress of the Parylene C layer to be 4.48 GPa and 20.88 MPa, respectively. Harder *et al* [39] studied the residual stress in the Parylene C film based on the load-deflection method and rotating tip strain gages. They found that 90% of the residual stress was attributed to the thermal stress in the Parylene C film. Furthermore, Shih *et al* [40] studied the yield strength of Parylene C film using the load-deflection tests with the balloon model. Hsu *et al* [41] proposed the chemical vapor deposition (CVD) method to coat the Parylene C thin film on the silicon wafer and evaluated the residual stress on a thin film by using the wafer bow method with the modified Stoney equation.

An exact analytical solution to relate the residual stress distribution to the curvature of an elastic bilayer system has been derived previously [42]. Based on this previous study, a Parylene C/silicon bilayer system has been constructed in this study to measure the bending curvature and calculate the residual stresses.

2. Experimental details

Figure 1 shows the schematic drawings of the processes to fabricate microcantilever beams. The starting materials were 4 inch, p-type double-side polished silicon wafers with ⟨1 0 0⟩

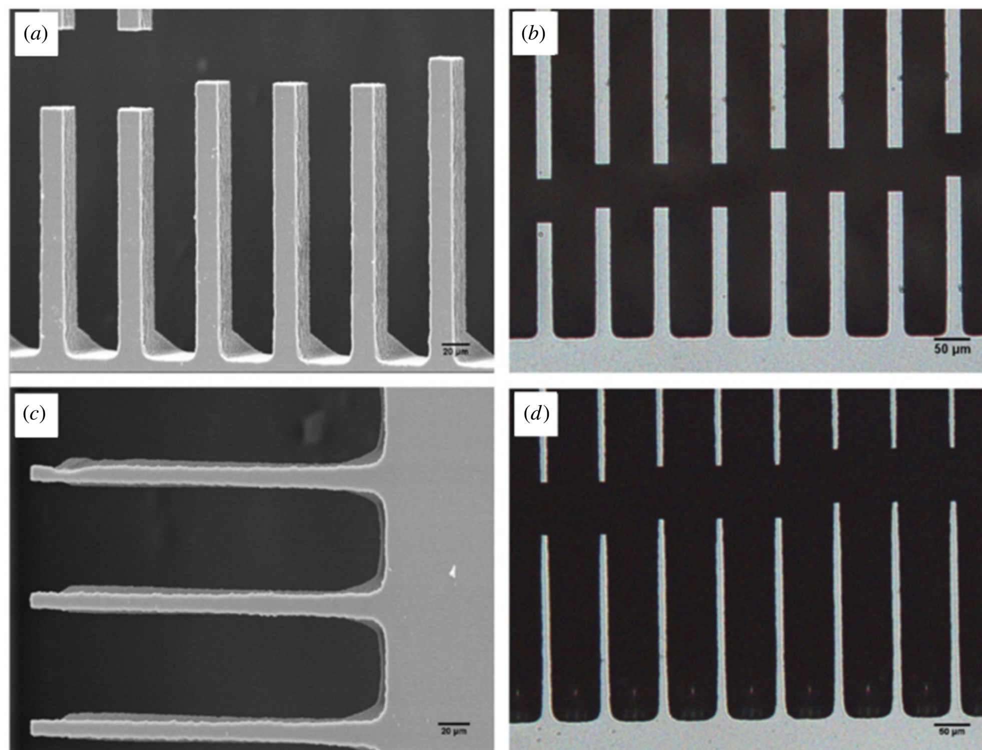

Figure 2. (*a*) SEM and (*b*) OM graphs of 21 μm thickness Si beam before Parylene C deposition. (*c*) SEM and (*d*) OM graphs of 27 μm thickness Si beam after Parylene C deposition.

orientation and 525 μm thickness. The Si wafer is shown in figure 1(*a*). After sulfuric acid pre-cleaning, 500 nm thick low stress silicon nitride (Si_3N_4) films were deposited on both sides of the Si wafer in a low-pressure CVD system by using a gas mixture of SiH_2Cl_2 and NH_3 at 850 °C (see figure 1(*b*)). Afterwards, FH 6400 positive photoresist was coated on the backside (see figure 1(*c*)) and rectangular patterns were transferred using lithography. In order to fabricate a series of silicon substrates, we applied the reactive ion etching (RIE) method to etch Si_3N_4 layer in SF_6/CHF_3 gas mixture and wet etched silicon in 45% KOH aqueous solution at 85 °C until the expected etching endpoint was reached (see figure 1(*d*)). Then, the RIE method was re-applied to remove the Si_3N_4 passive layer on the front side as shown in figure 1(*e*), and a double alignment exposure was used to transfer microcantilever beam patterns on Si substrates precisely (see figure 1(*f*)). For the purpose of manufacturing thicker microcantilever beams, structures were formed by inductively coupled plasma deep etching technology.

In order to prevent covering of Parylene C on all surfaces of the Si wafer, the backside of the patterned Si wafer was attached to another wafer of the same size. Then, a thickness of 2 μm Parylene C polymer thin film was deposited onto the composite wafer system as shown in figure 1(*g*). In this case, Parylene C dimer powders were loaded in a vacuum chamber and vaporized at 150 °C, and decomposed into chloro-*p*-xylene monomer at 690 °C. The gas monomers were then polymerized and deposited on the surface of structures at room temperature to form a continuous polymer thin film. Finally, two silicon wafers were separated. The wafer with microcantilever beam structures was obtained.

The thicknesses of both silicon beams and Parylene C film were measured by α-step surface profiler (Dektak 150, Veeco, USA). The deflections of microcantilever beams were measured by an interferometer (WYKO NT1100, Veeco, USA) under vertical scanning interferometry mode before and after Parylene C deposition. In addition, optical images as well as scanning electron micrographs were observed before and after Parylene C film deposition.

3. Results and discussion

The silicon microcantilever beams of various thicknesses between 15 and 45 μm were fabricated. The typical optical and SEM images of 21 and 27 μm thickness beams before and after Parylene C deposition are shown in figures 2(*a*)–(*d*). Narrower beams revealed uneven lateral etching rate along its length; thus the width at the root of beams is slightly wider than that at the end. During Parylene C deposition, the Parylene C film would cover the entire structure. As a result, a native Si wafer attached to the backside of the patterned wafer is required. After CVD of the Parylene C thin film, the native wafer was separated from the patterned one. Then, the Parylene C film of 2 μm thickness was formed uniformly on the structures without pinholes.

It is difficult to observe the difference in beam curvatures before and after Parylene C deposition using an optical microscope and SEM due to the high strength of single-crystal silicon. Hence, we applied the WYKO interferometer

Table 1. Radii of curvature r_A and r_B of beam before and after Parylene C deposition. r is the effective radius of curvature. The error is indicated by the value after ±.

h_s (mm)	$1/r_A$ (mm^{-1})	$1/r_B$ (mm^{-1})	$1/r$ (mm^{-1})	ΔT (°C)
15	$1.93 \times 10^{-3} \pm 2.63 \times 10^{-5}$	$-1.62 \times 10^{-4} \pm 1.31 \times 10^{-6}$	$2.10 \times 10^{-3} \pm 2.77 \times 10^{-5}$	48.98
19	$1.09 \times 10^{-3} \pm 1.43 \times 10^{-5}$	$-1.65 \times 10^{-4} \pm 6.06 \times 10^{-7}$	$1.26 \times 10^{-3} \pm 1.49 \times 10^{-5}$	48.18
24	$5.46 \times 10^{-4} \pm 1.70 \times 10^{-5}$	$-1.68 \times 10^{-4} \pm 6.30 \times 10^{-7}$	$7.14 \times 10^{-4} \pm 1.76 \times 10^{-5}$	44.33
27	$4.18 \times 10^{-4} \pm 5.19 \times 10^{-5}$	$-1.69 \times 10^{-4} \pm 1.85 \times 10^{-6}$	$5.88 \times 10^{-4} \pm 5.37 \times 10^{-5}$	46.56
45	$1.33 \times 10^{-5} \pm 4.39 \times 10^{-7}$	$-1.69 \times 10^{-4} \pm 2.14 \times 10^{-6}$	$1.83 \times 10^{-4} \pm 2.58 \times 10^{-6}$	41.26

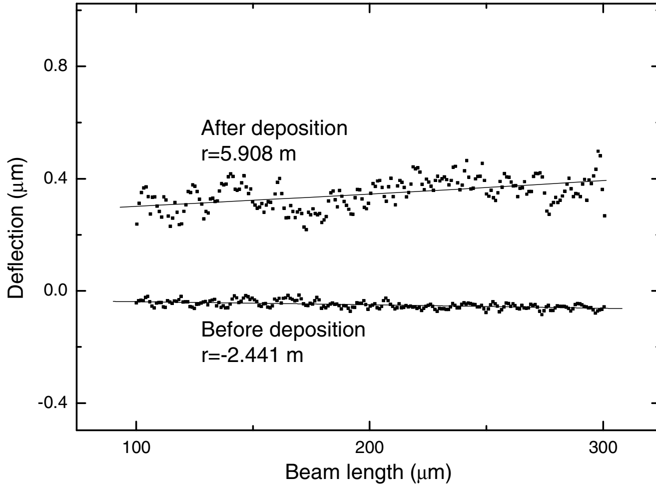

Figure 3. Deflection curves of the Si beam with thickness of 27 μm before and after Parylene C deposition.

Table 2. Young modulus, Poisson's ratio and coefficient of thermal expansion of silicon and Parylene C [31, 43].

Materials	E (GPa)	ν	α (10^{-6} °C^{-1})
Si	180	0.25	2.6
Parylene C	3.2	0.4	35

to investigate the variation of beam curvatures resulting from film deposition. The deflections along the length of the beam of 27 μm thickness before and after Parylene C film deposition are shown in figure 3. The change of deflection was observed with the deposited Parylene C film on the concave side; however, this side was convex before film deposition. Both the curvature and the standard deviation were obtained, and each datum listed in table 1 was averaged over three beams. Using these deflections and mechanical properties of Si and Parylene C listed in table 2 [31, 43], the residual stresses in microcantilevers could be analyzed using Hsueh and Lee's solution [42].

The system considered in this study is schematically shown in figure 4. The general solutions of elastic bilayer arising from bending curvature are expressed in the following [42]. The stresses in the substrate, σ_s, and in the film, σ_f, are

$$\sigma_s = B_s\varepsilon \quad \text{for} \quad -h_s \leqslant z \leqslant 0 \qquad (1a)$$

$$\sigma_f = B_f(\varepsilon - \Delta\varepsilon_f) \quad \text{for} \quad -0 \leqslant z \leqslant h_f, \qquad (1b)$$

where the biaxial modulus is equal to $E/(1-\nu)$ and E and ν are the Young modulus and the Poisson ratio, respectively. The

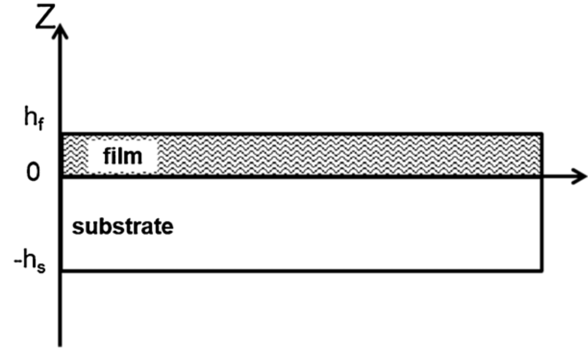

Figure 4. The schematic drawing of thin film/substrate systems in modeling.

total strain, ε, can be decomposed into the uniform strain, c, and the bending strain components, such that

$$\varepsilon = c + \frac{z - t_b}{r}, \qquad (2)$$

where z is the coordinate axis normal to the film/substrate plane, and $z = t_b$ is the location of the bending axis corresponding to zero bending strain. Note that the second term on the right-hand side of equation (2) denotes the bending strain component. The solutions subjected to the force equilibrium and moment equilibrium conditions are

$$c = \frac{B_f h_f \Delta\varepsilon}{B_f h_f + B_s h_s} \qquad (3)$$

$$t_b = \frac{B_f h_f^2 + B_s h_s^2}{2(B_f h_f + B_s h_s)} \qquad (4)$$

$$\frac{1}{r} = \frac{6B_f B_s h_f h_s (h_s + h_p)\Delta\varepsilon}{B_f^2 h_f^4 + B_s^2 h_s^4 + 2B_f B_s h_f h_s \left(2h_f^2 + 2h_s^2 + 3h_f h_s\right)}. \qquad (5)$$

Equation (5) can be used to calculate the mismatch strain if the radius of curvature, biaxial moduli and thicknesses of the films and substrates are given. The curvature is assigned to be positive when the film surface is convex. The average film stress is defined by

$$\overline{\sigma_f} = \frac{1}{h_f}\int_0^{h_f} \sigma_f \, \mathrm{d}z. \qquad (6)$$

Using equations (2)–(5) and substituting equation (1b) into equation (6), the average film stress is

$$\overline{\sigma_f} = \frac{-B_f B_s h_s \left(B_f h_f^3 + B_s h_s^3\right)\Delta\varepsilon}{B_f^2 h_f^4 + B_s^2 h_s^4 + 2B_f B_s h_f h_s \left(2h_f^2 + 2h_s^2 + 3h_f h_s\right)}. \qquad (7)$$

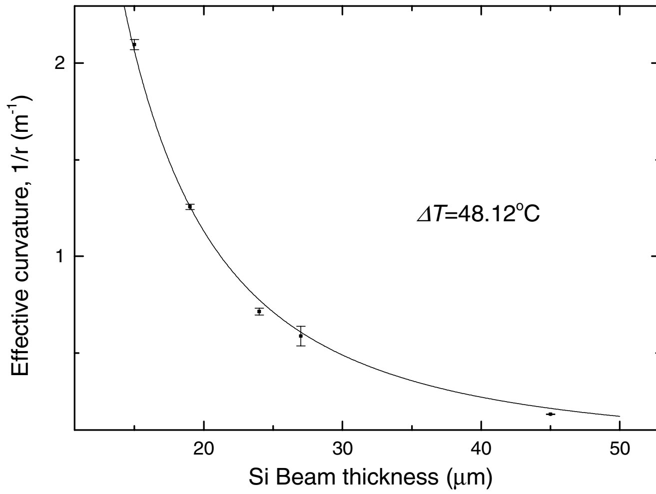

Figure 5. Effective curvature of the Si beam as a function of Si substrate thickness where the symbols are experimental data listed in table 1.

When the film thickness is very thin, equation (7) is reduced to Stoney's equation [33]

$$\sigma_{\mathrm{st}} = \frac{B_s h_s^2}{6 h_f r}. \quad (8)$$

Note that the sign of curvature in equation (8) is opposite to that in [38]. Considering the presence of the initial curvature of the cantilever before film deposition, the effective curvature $1/r$ induced by the film deposition process and the mismatch between the film and substrate is $1/r = 1/r_A - 1/r_B$, where $1/r_A$ and $1/r_B$ are the curvatures of microcantilever after and before film deposition, respectively. The effective curvature is used in equation (5) to calculate the residual stresses. From the data shown in table 1, the effective curvatures $1/r$ are obtained and re-plotted in figure 5. It shows that the curvature change decreases with the increasing thickness of the Si beam. Then the mismatch strain $\Delta\varepsilon$ and total strain ε can be calculated form equations (5) and (2), respectively. While the polymer film is amorphous [44], the lattice mismatch between the film and the substrate is not expected. However, although Parylene C deposition was performed in the chamber at room temperature, 25 °C, the monomer is formed at 690 °C and the temperature of the monomer gas flowing across the sample is expected to be higher than room temperature. Assuming no phase transition for Parylene C near room temperature, the curvature change is attributed to thermal mismatch which can be calculated using equation (5) with $\Delta\varepsilon$ replaced by $(\alpha_f - \alpha_s)\Delta T$, such that [14, 45]

$$\frac{1}{r} = \frac{6 B_f B_s h_f h_s (h_s + h_p)(\alpha_f - \alpha_s)\Delta T}{B_f^2 h_f^4 + B_s^2 h_s^4 + 2 B_f B_s h_f h_s \left(2h_f^2 + 2h_s^2 + 3 h_f h_s\right)}, \quad (9)$$

where α is the coefficient of thermal expansion (CTE); ΔT is temperature difference between the deposition temperature and 25 °C. Because all the samples were obtained from the same batch in the deposition chamber, the deposition temperature was expected to be the same for the substrate of different thicknesses. Thus the solid line in figure 5 was obtained using the best curve fitting to obtain the same

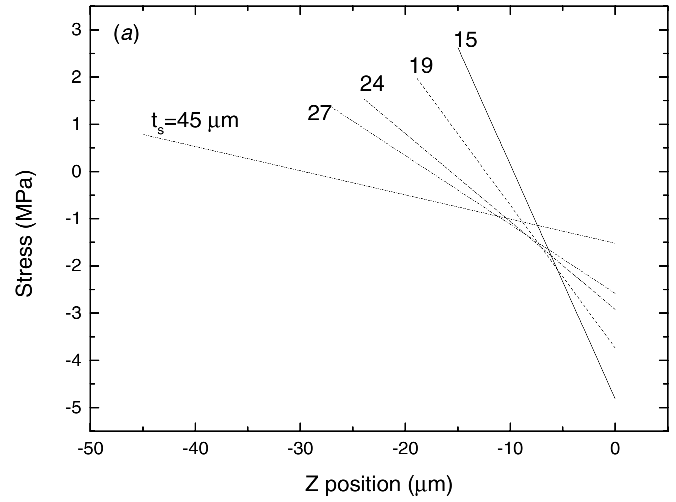

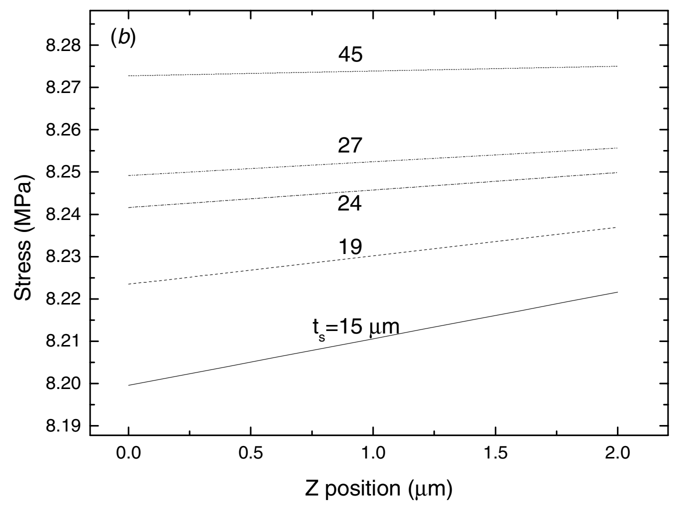

Figure 6. Residual stress distributions in (*a*) the Si substrate and (*b*) Parylene C film, respectively.

deposition temperature for different substrate thicknesses. Therefore, ΔT can be evaluated by fitting equation (9) to the experimental data for different substrate thicknesses in figure 5. As shown in figure 5, when $\Delta T = 48$ °C (i.e. $T = 73$ °C) is adopted in equation (9), good fitting is obtained. Using equations (1*a*) and (1*b*), the predicted stress distributions are plotted in figures 6(*a*) and (*b*). The stress is linear through the thickness in each layer and discontinuous at the interface between Si and Parylene C. In addition, the stress gradient in the film is different from that in the substrate due to the different elastic constants. Note that the value of stress is positive when tensile and negative when compressive. Thus, the Parylene C film is subjected to tension, while the Si substrate is subjected to combination of tension and compression. However, a net negative force exists in the Si layer which results from its lower CTE. It is also observed that the tensile residual stresses in the Parlyene C film decreases with decreasing substrate thickness. This is reasonable because the stress magnitude in the film increases with decreasing ratio of film thickness to substrate thickness. In all cases, the residual stress in Parylene C coating is of the order of MPa. Hence, measurements of

Table 3. Residual stresses and positions of neutral axes.

t_s (mm)	t_f/t_s	$\bar{\sigma}_f$ (MPa)	σ_{st} (MPa)	$\frac{1+\gamma\delta^3}{1+\delta}$	t_b (μm)	t_n (μm)
15	0.13	8.21	9.30	0.882	−7.47	−9.67
19	0.11	8.23	9.10	0.905	−9.48	−12.36
24	0.08	8.25	8.94	0.923	−11.98	−16.01
27	0.07	8.25	8.86	0.931	−13.48	−17.83
45	0.04	8.27	8.64	0.957	−22.48	−30.88

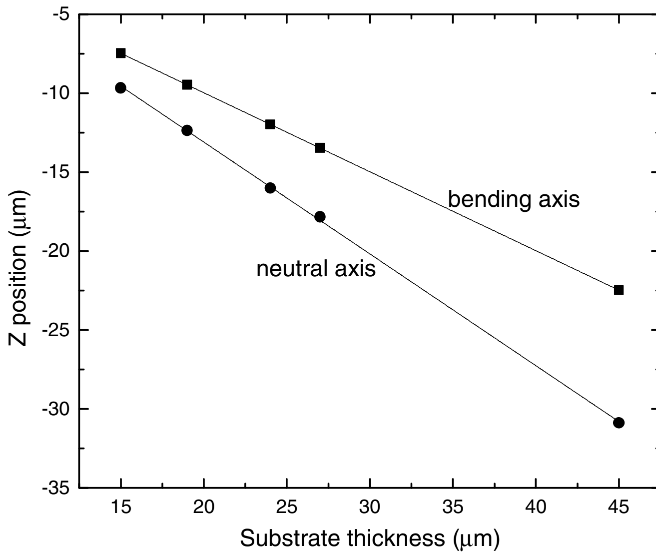

Figure 7. Positions of neutral and bending axes as functions of the substrate thickness for film thickness of 2 μm.

deflection can be used to characterize the residual stress in coatings that have a low stress level.

The average residual film stresses were calculated using equations (1) and (8), respectively, and listed in table 3. Results obtained from Stoney's equation are always greater than the values calculated by equation (1) and can be corrected by the factor $(1+\gamma\delta^3)/(1+\delta)$. Here, γ designates the ratio of film biaxial modulus to substrate biaxial modulus and δ is the ratio of film thickness to substrate thickness. It can be seen from table 3 that the correction factor is unity when film thickness is infinitesimal, and the correction factor increases with decreasing t_f/t_s values. The residual stress of 8.2 MPa of the Parylene C film in this study is lower than 20.8 MPa obtained by Yang *et al* [38]. They found that squeegee coating technique produced a more uniform Parylene C film than spin coating ones. Harder *et al* [39] measured the residual stress increasing from 33.8 to 44.4 MPa with increasing annealing temperature in the range from 140 to 180 °C. Their stress values are also greater than ours because of the process temperature in this study at 73 °C. Hsu *et al* [41] observed the residual stress of as chemical-deposited Parylene C film of 1.56 MPa. After annealing at 150 °C for 20 min, their tensile stress increases (<15 MPa) that covers our residual stress value. The positions of bending axis, t_b, and neutral axis, t_n, are located in the Si substrate and plotted in figure 7. The bending axis and the neutral axis are located, respectively, at about half the substrate thickness and two-third the substrate thickness underneath the film/substrate interface.

It should be noted that only coating of Parylene C film on the front side of the silicon wafer was considered in the above analysis. The issue of coating of Parylene C on the sidewalls and backside of cantilever beam is worth addressing because of the characteristics of conformal coating of Parylene C, which is known to deposit into small gaps with high aspect ratios. Using Scanning Auger Nanoprobe and SEM, Parylene C was verified to appear on both sidewalls and backside of the wafer. Because the front side of cantilever beams was faced to the reactant gases, Parylene C on sidewalls was expected to be symmetric on the two sides. Even if the Parylene C coated on sidewalls is not symmetric, the direction of the corresponding deflection is normal to that from Parylene C coating on the front side and does not affect residual stress analysis from the bending curvature. On the other hand, although Parylene C could coat the backside of the wafer, it is reasonable to assume that its thickness is limited by the gap between the two wafers. With the rigid contact between two wafers, the gap is determined by the surface roughness of the wafer. While the surface roughness of wafer was measured to be 5.4 nm, the Parylene C film deposited on the backside is expected to be less than 10. 8 nm that is much smaller than 2 μm thickness of Parylene C deposited on the front side. Thus, the effect of film coating on the backside could be neglected in our case. In addition, if the coating thickness on the backside could be measured and could not be ignored, the model developed in [42] still could be applied because it was derived for a multilayer system.

4. Conclusions

The residual stresses in the Parylene C film and Si substrate bilayer system measured by the microcantilever method were investigated. Parylene C films of 2 μm thickness were deposited on Si beams with various thicknesses in the range from 15 to 45 μm. SEM images showed an ideal pinhole-free film on the top of beams. The change of deflection is observed with Parylene C on the concave side after deposition that results from a higher thermal expansion coefficient of Parylene C than Si. Although Parylene C deposition was performed in the chamber at room temperature, 25 °C, the temperature of monomer gas flowing across the sample could be higher than 25 °C and it is estimated to be 73 °C based on the fitting of the curvature versus substrate thickness relation between the measurements and analytical solutions. The stress is linear through the thickness in each layer and discontinuous at the interface. Parylene C is subjected to tension and the Si substrate is subjected to the combination of tension and compression. The correction factor $(1+\gamma\delta^3)/(1+\delta)$ increases with decreasing of t_f/t_s values.

Acknowledgment

This work was financially supported by the National Science Council, Taiwan.

References

[1] Butt H J 1996 *J. Colloid Interface Sci.* **180** 251–60
[2] Lang H P *et al* 1999 *Anal. Chim. Acta* **393** 59–65
[3] Fritz J, Baller M K, Lang H P, Rothuizen H, Vettiger P, Meyer E, Guntherodt H J, Gerber C and Gimzewski J K 2000 *Science* **288** 316–8
[4] O'Mahony C, Hill M, Duane R and Mathewson A 2003 *J. Micromech. Microeng.* **13** S75–80
[5] Chaterjee S and Pohit G 2009 *J. Sound Vib.* **322** 969–86
[6] Sadeghian H and Rezazadeh G 2009 *Commun. Nonlinear Sci. Numer. Simul.* **14** 2807–16
[7] Wang B, Zhou S, Zhao J and Chen X 2011 *J. Micromech. Microeng.* **21** 027001
[8] Pamidighantam S, Puers R, Baert K and Tilmans H A C 2002 *J. Micromech. Microeng.* **12** 458–62
[9] Chen R T, Nguyen H and Wu M C 1999 *IEEE Photon. Technol. Lett.* **11** 1396–8
[10] Wolffenbuttel R F 2005 *J. Micromech. Microeng.* **15** S145–52
[11] Zhang Y, Zhang Y and Marcus R B 1999 *J. Microelectromech. Syst.* **8** 43–9
[12] Rokni H and Lu W 2013 *J. Microelectromech. Syst.* **22** 553–9
[13] Fang W and Wickert J A 1999 *J. Micromech. Microeng.* **6** 301–9
[14] Hsueh C-H 2002 *J. Appl. Phys.* **91** 9652–6
[15] Koch R 1999 *J. Phys.: Condens. Matter* **6** 9519–50
[16] Mayr S G and Samwer K 2001 *Phys. Rev. Lett.* **87** 036105
[17] Nix W D and Clemens B M 1999 *J. Mater. Res.* **14** 3467–73
[18] Cammarata R C, Trimble T M and Srolovitz D J 2000 *J. Mater. Res.* **15** 2468–74
[19] Fang W and Wickert J A 1995 *J. Micromech. Microeng.* **5** 276–81
[20] Min Y H and Kim Y K 2000 *J. Micromech. Microeng.* **10** 314–21
[21] Zhang T-Y, Lee S, Guido L J and Hsueh C-H 1999 *J. Appl. Phys.* **85** 7579–86
[22] Gianchandani Y B and Najafi K 1996 *J. Microelectromech. Syst.* **5** 52–8
[23] Ericson F, Greek S, Soderkvist J and Schweitz J A 1997 *J. Micromech. Microeng.* **7** 30–6
[24] Guckel H, Burns D, Rutigliano C, Lovell E and Choi B 1999 *J. Micromech. Microeng.* **2** 86–95
[25] Guckel H, Randazzo T and Burns D 1985 *J. Appl. Phys.* **57** 1671–5
[26] Zhang L, Uttamchandani D and Culshaw B 1991 *Sensors Actuators* A **29** 79–84
[27] Zou Q, Li Z and Liu L 1995 *Sensors Actuators* A **48** 137–43
[28] Meng E, Li P-Y and Tai Y-C 2008 *J. Micromech. Microeng.* **18** 045004
[29] Wright D, Rajalingam B, Karp J M, Selvarasah S, Ling Y, Yeh J, Langer R, Dokmeci M R and Khademhosseini A 2008 *J. Biomed. Mater. Res.* A **85** 530–8
[30] Bienkiewicz J 2006 *Med. Devices Technol.* **17** 10–11
[31] Noh H-S, Moon K-S, Cannon A, Hesketh P J and Wong C P 2004 *J. Micromech. Microeng.* **14** 625–31
[32] Schmidt E M, Bak M J and Christensen P 1995 *J. Neurosci. Methods* **62** 89–92
[33] Stoney G G 1909 *Proc. R. Soc. Lond.* A **82** 172–5
[34] Röll K 1976 *J. Appl. Phys.* **47** 3224–9
[35] Benabdi M and Roche A A 1997 *J. Adhes. Sci. Technol.* **11** 281–99
[36] Huang S and Zhang X 2006 *J. Micromech. Microeng.* **16** 382–9
[37] Lin Y Y 2000 *J. Electron. Packag.* **122** 267–73
[38] Yang X, Grosjean C and Tai Y C 1999 *J. Microelectromech. Syst.* **8** 393–402
[39] Harder T A, Yao T J, He Q, Shih C Y and Tai Y C 2002 *15th IEEE Int. Conf. on Micro Electro Mechanical Systems (Las Vegas)* pp 435–8
[40] Shih C Y, Harder T A and Tai Y C 2004 *Microsyst. Technol.* **10** 407–11
[41] Hsu J-M, Kammer S, Jung E, Rieth L, Normann R A and Solzbacher F 2007 *3rd Int. Conf. on Multi-Mater. Micro Manufac. (Borovets, Bulgaria)* pp 355–8
[42] Hsueh C-H and Lee S 2002 *J. Appl. Phys.* **91** 2760–5
[43] Abadal G *et al* 2001 *Nanotechnology* **12** 100–4
[44] Fukuda K, Suzuki T, Kumaki D and Tokito S 2012 *Phys. Status Solidi* **209** 2073–7
[45] Hsueh C-H, Lee S and Lin H-Y 2006 *Composites* B **37** 1–9